

AD-A130 489

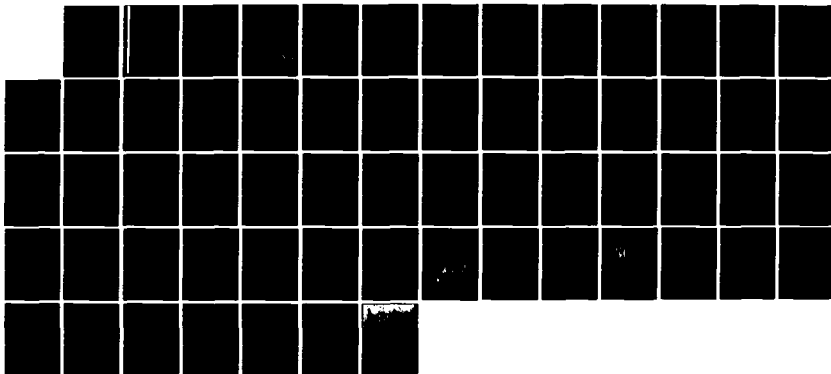
SHORT-WAVELENGTH ION WAVES UPSTREAM OF THE EARTH'S BOW
SHOCK(U) IOWA UNIV IOWA CITY DEPT OF PHYSICS AND
ASTRONOMY S A FUSELIER ET AL. 02 JUN 83
U. OF IOWA-83-21 N00014-76-C-0016

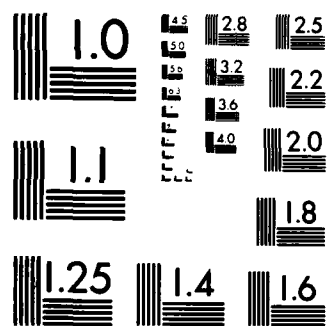
1/1

UNCLASSIFIED

F/G 20/3

NL





MICROCOPY RESOLUTION TEST CHART
NATIONAL BUREAU OF STANDARDS-1963-A

10

ADA 130489

SHORT-WAVELENGTH ION WAVES UPSTREAM
 OF THE EARTH'S BOW SHOCK
 by
 S. A. Fuselier and D. A. Gurnett



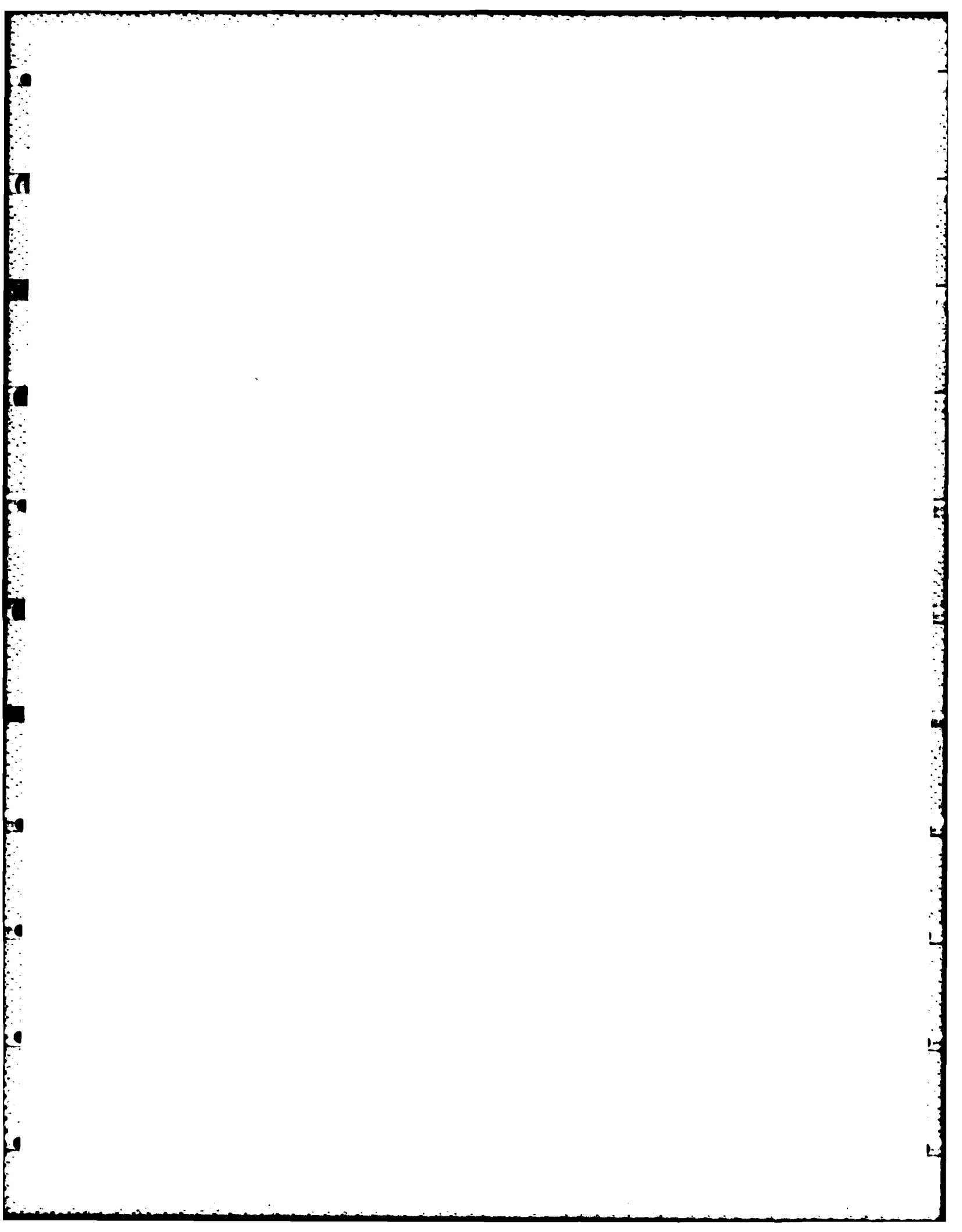
DTIC
 ELECTRONIC
 JUL 10 1983
 S
 B

DTIC FILE COPY

Department of Physics and Astronomy
THE UNIVERSITY OF IOWA

Iowa City, Iowa 52242

DISTRIBUTION STATEMENT A
 Approved for public release;
 distribution unlimited



U. of Iowa 83-21

SHORT-WAVELENGTH ION WAVES UPSTREAM
OF THE EARTH'S BOW SHOCK

by

S. A. Fuselier and D. A. Gurnett

June, 1983

Department of Physics and Astronomy
The University of Iowa
Iowa City, IA 52242

DTIC
ELECTE
S JUL 20 1983 D
B

This work was supported by the National Aeronautics and Space Administration through Contract NAS5-26829 with Goddard Spaceflight Center and Grant NGL-16-001-043 with NASA Headquarters, and the Office of Naval Research.

DISTRIBUTION STATEMENT A

Approved for public release;
Distribution Unlimited

UNCLASSIFIED

SECURITY CLASSIFICATION OF THIS PAGE (When Data Entered)

REPORT DOCUMENTATION PAGE		READ INSTRUCTIONS BEFORE COMPLETING FORM
1. REPORT NUMBER U. of Iowa 83-21	2. GOVT ACCESSION NO. AD-A130489	3. RECIPIENT'S CATALOG NUMBER
4. TITLE (and Subtitle) SHORT-WAVELENGTH ION WAVES UPSTREAM OF THE EARTH'S BOW SHOCK		5. TYPE OF REPORT & PERIOD COVERED Progress, June 1983
		6. PERFORMING ORG. REPORT NUMBER
7. AUTHOR(s) S. A. FUSELIER and D. A. GURNETT		8. CONTRACT OR GRANT NUMBER(s) N00014-76-C-0016
9. PERFORMING ORGANIZATION NAME AND ADDRESS Department of Physics and Astronomy The University of Iowa Iowa City, IA 52242		10. PROGRAM ELEMENT, PROJECT, TASK AREA & WORK UNIT NUMBERS
11. CONTROLLING OFFICE NAME AND ADDRESS Electronics Program Office Office of Naval Research Arlington, VA 22217		12. REPORT DATE 02 June 1983
		13. NUMBER OF PAGES 56
14. MONITORING AGENCY NAME & ADDRESS (if different from Controlling Office)		15. SECURITY CLASS. (of this report) UNCLASSIFIED
		15a. DECLASSIFICATION/DOWNGRADING SCHEDULE
16. DISTRIBUTION STATEMENT (of this Report) Approved for public release; distribution is unlimited		
17. DISTRIBUTION STATEMENT (of the abstract entered in Block 20, if different from Report)		
18. SUPPLEMENTARY NOTES To be published in <u>J. Geophys. Res.</u>		
19. KEY WORDS (Continue on reverse side if necessary and identify by block number) Electrostatic Waves Interplanetary Magnetic Field Bow Shock		
20. ABSTRACT (Continue on reverse side if necessary and identify by block number) (See following page)		

DD FORM 1 JAN 73 1473

EDITION OF 1 NOV 65 IS OBSOLETE
S/N 0102-LF-014-6601

UNCLASSIFIED

SECURITY CLASSIFICATION OF THIS PAGE (When Data Entered)

ABSTRACT

The identification and explanation of short wavelength antenna interference effects observed in spacecraft plasma wave data have provided an important new method of determining limits on the wavelength, direction of propagation, and Doppler shift of short wavelength electrostatic waves. Using the ISEE-1 wideband electric field data, antenna interference effects have been identified in the ion waves upstream of the Earth's bow shock. This identification implies that wavelengths of the upstream ion waves are shorter than the antenna length. The interference effects also provide new measurements of the direction of propagation of the ion waves. The new measurements show that the wave vectors of the ion waves are not parallel to the interplanetary magnetic field (IMF) as previously reported. The direction of propagation does not appear to be controlled by the IMF. In addition, analysis of the Doppler shift of the short wavelength ion waves has provided a measurement of the dispersion relation, $\omega(k)$. The upper limit on the rest frame frequency was found to be on the order of the ion plasma frequency. At this frequency, the wavelength is on the order of a few times the Debye length. The results of this study now provide strong evidence that the ion waves in the upstream region are Doppler-shifted ion acoustic waves.

<input checked="" type="checkbox"/>
<input type="checkbox"/>
<input type="checkbox"/>



Distribution/	
Availability Codes	
Dist	Avail and/or Special
A	

I. INTRODUCTION

Electrostatic waves in the region upstream of Earth's bow shock with frequencies ranging from 0 to 10 kHz were first identified by Scarf et al. [1970]. Scarf et al. reported that the electrostatic waves were associated with energetic ion beams produced in the bow shock. Gurnett and Frank [1978], using wave data from the IMP 6 spacecraft, made the first measurements of the wavelength of the upstream electrostatic waves. These measurements gave the first indication that the electrostatic waves had wavelengths on the order of a few times the Debye length. Based on the short wavelengths and other characteristics similar to the ion acoustic waves observed in the solar wind far from Earth by the Helios spacecraft [Gurnett and Anderson, 1977], it was concluded that the upstream electrostatic waves were ion acoustic waves Doppler-shifted from below the ion plasma frequency to frequencies of 1 to 10 kHz by the motion of the solar wind. The term "ion waves" was first used by Rodriguez [1981], who questioned the short wavelength characteristic and suggested instead that a Buneman-like instability was responsible for producing the waves. Gary [1978 and 1981] suggested that ion waves in the upstream region be called ion acoustic-like waves because in his theory the waves were generated by an ion beam mode which is technically different from the ion acoustic mode. Lemons et al. [1979] considered both a beam-plasma interaction and an

ion-electron drift instability but was not successful in demonstrating an instability that would generate field aligned ion acoustic waves using typical upstream plasma parameters. Other instabilities such as the ion density gradient instability [Wu et al., 1982] have also been suggested. At the present time, the exact mechanism for producing upstream ion waves remains unknown.

A more recent observational study of the ion waves has been done by Anderson et al. [1981] using data from the ISEE-1 and -2 spacecraft. By analyzing plasma wave electric field data, Anderson et al. confirmed that the wavelength of the ion waves in the upstream region was between 30 and 215 meters and concluded that the direction of propagation was primarily parallel to the ambient magnetic field. Using wave and particle data, Anderson et al. verified that ion waves in the upstream region are associated with reflected ion flux enhancements. Based on these observations, it was concluded by Anderson et al., in agreement with Gurnett and Frank [1978], that the ion waves observed were probably ion acoustic waves Doppler-shifted into the 1 to 10 kHz frequency range by the motion of the solar wind.

The purpose of this work is to determine the wavelength and propagation direction of the ion waves using an independent and much more powerful method. In addition, the Doppler shift of the ion waves is determined and the rest frame frequency is obtained as a function of the magnitude of the wave vector.

The wideband wave data used in this study came from the wideband receivers in the University of Iowa Plasma wave experiment on ISEE-1

and -2. More detailed information on the plasma wave instruments can be found in Gurnett et al. [1978]. Both spacecraft have essentially identical wideband receivers. The primary difference in the two instruments is the electric antenna. The electric dipole antenna on ISEE-1 has a tip-to-tip length of 215 meters, whereas on ISEE-2 the tip-to-tip length is 30 meters.

II. ANTENNA INTERFERENCE EFFECTS

The method of determination of the wavelength, direction of propagation, and Doppler shift involves the study of spin modulated interference patterns in the wideband data from ISEE-1. These interference patterns were first identified by Anderson et al. [1982] in wideband data from the outer magnetosheath, where waves very similar to the upstream ion waves are observed. The interference patterns have a characteristic frequency-time spectrum first described by Anderson et al. as "festoon-shaped" emissions.

In this work, spin modulated interference patterns are identified in wideband frequency-time spectrograms from the region upstream of the bow shock. An example of the interference pattern observed is presented in Figure 1. The lower panel in Figure 1 is a frequency-time spectrogram from the ISEE-1 wideband receiver for December 24, 1977. ISEE-1 at this time was located in the upstream region at a distance of about $22 R_E$ and a magnetic local time of about 6.1 hours. The periodic change in frequency in the lower panel of Figure 1 from $17^h 23^m 48^s$ to $17^h 23^m 50^s$ occurs at one-half the spacecraft rotation period. The basic frequency-time pattern evident in the wideband spectrum is illustrated in the top panel of Figure 1.

An explanation of the spectral features of short wavelength electrostatic waves was given by Gallagher [1982]. Gallagher studied ion

waves in the outer magnetosheath, where interference patterns very much like those found in Figure 1 were identified. Gallagher identified the interference patterns in the electric field data as an antenna effect caused by the presence of electrostatic waves with wavelengths shorter than the spacecraft electric field antenna.

To aid in understanding these interference effects it is useful to review the important features of the response of an electric dipole antenna to an electrostatic plane wave, following the development given by Gallagher [1982]. This development is similar to the theory developed by Temerin [1979] to explain antenna interference effects observed in low altitude satellites.

The potential between two points in space is given by

$$\phi = -\int \vec{E} \cdot d\vec{s} \quad . \quad (1)$$

The electric field of a plane, electrostatic wave, confined to the x - z plane, is given by

$$\vec{E} = (E_x \hat{x} + E_z \hat{z}) e^{i\vec{k} \cdot \vec{r} - i\omega t} \quad .$$

If it is assumed for simplicity that the antenna is rotating in the x - y plane then $d\vec{s} = d\rho \hat{\rho}$, $\vec{E} \cdot d\vec{s} = E_x \cos \phi d\rho$, and $\vec{k} \cdot \vec{r} = k_x \rho \cos \phi$, where ϕ is the azimuthal angle. The relevant geometry for this calculation is

illustrated in Figure 2. Integrating Equation 1 between two points $-\ell/2$ to $\ell/2$ gives

$$\phi = \frac{-2(E_x \cos \phi) \sin(k_x \frac{\ell}{2} \cos \phi) e^{-i\omega t}}{k_x \cos \phi} \quad (2)$$

The potential measured by the spacecraft depends on how the antenna responds to the electrostatic wave. If the antenna responds capacitively to the electrostatic wave and the capacitance per unit length along the antenna is constant, then the potential measured by the instrument is the average potential over one element of the antenna,

$$\bar{\phi} = \int_0^L \phi \, d\ell / \int_0^L d\ell \quad (3)$$

Upon integration and using the identity, $1 - \cos \alpha = 2 \sin^2 \alpha/2$, the average potential of the antenna element is

$$\bar{\phi} = \frac{-8(E_x \cos \phi) \sin^2(\frac{k_x L \cos \phi}{4}) e^{-i\omega t}}{L (k_x \cos \phi)^2} \quad (4)$$

The measured voltage, V_m , is the root mean square of the average potential. Squaring Equation 4, averaging over one wave period, and taking the square root gives

$$V_m = \frac{1}{\sqrt{2}} \frac{L}{2} |E_x \cos \phi| \frac{\sin^2 x}{x^2}, \quad (5)$$

where $x = \frac{k_x L \cos \phi}{4}$.

For waves with wavelengths $\lambda \gg L$ the $\sin^2 x/x^2$ term in Equation 5 approaches unity and the usual cosine spin modulation in the power spectrum is obtained. If $\lambda \sim L$ then the $\sin^2 x/x^2$ term produces a characteristic interference pattern that can be observed in the wide-band data. To more thoroughly understand this term it is useful to determine the minimum and maximum condition for the measured voltage. The minimum in the measured voltage occurs when $\sin^2 x/x^2$ is zero. This condition is met when

$$\frac{k_x L \cos \phi}{4} = m \frac{\pi}{2}, \quad m = 2, 4, \dots \quad (6)$$

The nulls indicated by Equation 6 can be used to determine the wavelength of the ion waves. A simple explanation of the characteristic shape of a typical interference pattern can be seen by rewriting Equation 6 as follows

$$Lk_x = \frac{2m\pi}{\cos \phi} \quad (7)$$

For a fixed antenna position, from Equation 7, the condition for a minimum, ($V_m = 0$) is met when an integer number of wavelengths are projected onto the antenna. The average potential will be zero for an integer number of projected wavelengths. Since the Doppler shift gives a correspondence between the frequency and the wave vector via the relation $\omega' = \omega_0 + \vec{k} \cdot \vec{v}_{sw}$, where ω' is the frequency measured in the frame of the spacecraft, ω_0 is the frequency in the rest frame of the plasma, and \vec{v}_{sw} is the solar wind velocity, any projected wave vector which gives zero averaged power corresponds to a null at a certain frequency in the wideband data. As the antenna rotates and the angle ϕ between the projected wave vector and the antenna approaches $\pm \pi/2$, larger and larger projected wave vectors are required to meet the minimum condition. The pattern repeats every one-half spacecraft rotation. The interference pattern is thus seen to provide the direction of the wave vector projected onto the spin plane of the antenna.

The maximum measured voltage can also be used to determine the wave vector direction projected onto the spin plane. The maximum measured voltage occurs when $\sin^2 x$ in Equation 5 is a maximum or when

$$\frac{k_x L \cos \phi}{4} = \frac{m\pi}{2}, \quad m = 1, 3, 5, \dots \quad (8)$$

It is important to realize that studying the interference patterns does not give any information about the component of the wave vector perpendicular to the spin plane. This information is lost when the dot product $\vec{E} \cdot d\vec{s}$ is taken to find the potential. This lack of

information must be carefully considered when making wavelength estimations and measurements of the propagation direction. Fortunately, for the ISEE data the perpendicular component of the wave vector does not enter into the calculation of the Doppler shift because the spacecraft spin axis is oriented perpendicular to the plasma flow velocity so that

$$k_z V_{sw_z} = 0.$$

III. QUALITATIVE CHARACTERISTICS

Without making detailed calculations, much information about ion waves in the upstream region can be obtained from the identification and study of the interference patterns. The qualitative results in this section help further the understanding of the underlying physical processes that cause the interference patterns. In addition, some fundamental processes of waves in plasmas such as Doppler shift and Debye length are simply illustrated.

The first characteristic obtained from studying the wideband data is an estimation of the wavelengths of the upstream ion waves. To estimate the wavelengths one makes use of the fact that the ISEE-1 and -2 spacecraft are in nearly identical Earth orbits and on occasion are close enough together to observe nearly simultaneous upstream ion events. As pointed out in the introduction, the wideband receivers on ISEE-1 and -2 are essentially identical but the lengths of the electric dipole antennas on the spacecraft are different. As a result, differences in the wideband data for near simultaneous upstream ion events will be a result of the difference in the antenna response of the 215 meter dipole antenna on ISEE-1 as compared to the response of the 30 meter dipole antenna on ISEE-2.

As an example of the differences in the wave data, in Figure 3 the wideband frequency-time spectrograms are displayed for November 8, 1977

at 20^h 22^m U.T. The spacecraft location for the event was 17 R_E and 8.4^h magnetic local time. The separation of the two spacecraft was about 300 km. Protons travelling away from the bow shock at about solar wind speed take about one second to travel between the spacecraft, so the events occur nearly simultaneously at the two spacecraft. Comparing the two spectrograms in Figure 3 shows a general agreement in the change in frequency with time. The frequency-time wideband data for ISEE-1 clearly show evidence of interference patterns. For example, note the interference patterns centered around 20^h 22^m 15^s in the ISEE-1 wideband data. This observation of interference patterns in the ISEE-1 wideband data implies that the wavelength in the spin plane must be less than or approximately equal to 215 meters, the length of the ISEE-1 antenna.

In contrast, no interference patterns are evident in the ISEE-2 spectrogram. The absence of interference patterns in the ISEE-2 data is an indication that the wavelength in the spin plane is longer than 30 meters, the length of the electric antenna on ISEE-2. This lower limit on the wavelength is in agreement with an approximate calculation of the Debye length for waves in the upstream region. The minimum wavelength allowed in a plasma is usually taken to be $\lambda_{\min} \approx 2\pi \lambda_{De}$, which for the example in Figure 3 places λ_{\min} at about 41 meters [Anderson et al., 1981]. This minimum wavelength is longer than the antenna length on ISEE-2, so interference patterns in the wideband data from this spacecraft should not be a common occurrence.

The lack of information on the component of the wave vector perpendicular to the spin plane means that one can only measure the

wavelength in the spin plane and not the actual wavelength of the ion waves. However, the fact that interference patterns are frequently observed in the wideband data from ISEE-1 implies that the typical wavelength is not longer than the length of the ISEE-1 antenna. If the typical wavelength was always much longer than the antenna, interference effects would not be observed no matter what the wave vector direction.

The qualitative evaluation presented above indicate a wavelength between 30 and 215 meters for the ion waves. Anderson et al. [1981] compared the electron field spectra for ISEE-1 and ISEE-2 and noted that the ion wave spectral densities on ISEE-2, the spacecraft with the shorter antenna, were greater than those on ISEE-1. From this observation, Anderson et al. concluded that ion waves in the upstream region have wavelengths between 30 and 215 meters, in agreement with this present study.

Another characteristic of the upstream ion waves is that the direction of the wave vector does not change as a function of frequency. One can show that the wave vector does not change as a function of frequency using the interference patterns observed in the wideband data. Consider in Figure 4 the interface between the two adjacent interference patterns, indicated by an arrow at about 6^h 44^m 17.3^s. The antenna at this time is oriented exactly perpendicular to the spin plane projected wave vector. The null in the emission for all frequencies at 6^h 44^m 17.3^s indicates that the antenna is perpendicular to all spin plane projected wave vectors. This result indicates that the azimuthal directions of the wave vectors are the same for all

frequencies. Although no information can be obtained on the possible changes in k_z as a function of frequency, it seems almost certain that the polar direction must also be independent of frequency. Otherwise, one would have to assume that the wave vector distribution is somehow determined by the z-axis orientation of the spacecraft.

In addition to wavelength determinations and wave vector direction considerations, the effects of the Doppler shift due to the motion of the solar wind can be illustrated. A good example of the effects of Doppler shift on the interference patterns occurs on November 23, 1977 at 8^h 19^m U.T. and is illustrated in Figure 5. On November 23, the ISEE-1 spacecraft was located in the upstream region at a magnetic local time of about 9 hours and a radial distance of about 20 R_E . Starting from about 8^h 19^m 14^s U.T. the interference patterns retain their shape but shift downward in frequency as time progresses. This downshift can be understood by first considering the Doppler shift equation,

$$\omega'(\vec{k}) = \omega_0(\vec{k}) + \vec{k} \cdot \vec{v}_{sw} \quad , \quad (9)$$

which relates a given wave vector to a Doppler-shifted frequency. If the direction, or magnitude of the wave vector, or the solar wind velocity changes, then there is a change in the Doppler-shifted frequency. Most probably the frequency variations are caused by changes in the wave vector because the solar wind magnitude and direction are usually constant on time scales of seconds [W. C. Feldman, personal

communication, 1983]. Detailed analysis of the wave vector direction, which will be described in the next section, indicates that the direction of the wave vector with respect to the solar wind velocity shifted from 8^h 19^m 14^s to 8^h 19^m 18.4^s. This shift in direction caused a change in the Doppler shift for all wavelengths present. The fact that the Doppler-shifted frequency can change over a period of a few seconds is an indication that the wave vector of the electrostatic waves is highly variable.

A final example of characteristics of the ion waves deals with how the spectrum of the electric field emissions changes when ISEE-1 enters the outer magnetosheath. A good example of the change in the interference patterns is presented in Figure 6. In this figure the orbit of ISEE-1 projected into the equatorial plane is combined with examples of the wideband data from the upstream region at 6^h 56^m and from the outer magnetosheath at 9^h 25^m. The ion waves observed in the outer magnetosheath on this day were studied in detail by Gallagher [1982] and have the same characteristics as the ion waves observed in the upstream region. A major difference in the appearance of the wideband data is that the magnetosheath ion waves are only Doppler shifted to 4 kHz. The ion waves in the upstream region on the same pass show Doppler shifts up to 10 kHz. This difference in Doppler shift can be easily understood because the two regions of interest have different plasma flow velocities and directions. The solar wind velocity on November 22, 1977, is on the order of 300 km/sec [W. C. Feldman, personal communication, 1983], and is directed almost antisunward. An

estimate of the minimum wavelength allowable using an electron temperature of $1.6 \times 10^5 \text{K}$ [W. C. Feldman, personal communication, 1983] is about 50 meters. This minimum wavelength results in a maximum Doppler shift from zero rest frame frequency of about 7 kHz. This upper cutoff frequency should be compared with the wideband data in Figure 6 at 8^h 56^m. The upper cutoff frequency is not in exact agreement with Figure 6 because the electric field emissions are observed at frequencies as high as 10 kHz; however, the agreement is still reasonably good. One reason there is not exact agreement is that the rest frame frequency will be shown in the next section to be greater than zero. In the magnetosheath for the same day at 9^h 25^m the bulk flow velocity was around 160 km/sec and the minimum wavelength from typical plasma parameters for that region was around 36 meters [Gallagher, 1982]. Furthermore, in the magnetosheath there was a large shift in the direction of the bulk plasma flow velocity away from the antisunward direction. These approximate parameters result in a maximum Doppler shift on the order of 4 kHz. This upper cutoff frequency should be compared with the fact that no emissions are observed above 4 kHz in Figure 6 at 9^h 25^m. The above comparison shows good relative agreement with the Doppler shift character of the ion waves. In the next section more detailed analysis of the direction of propagation and Doppler shift of the waves in the upstream region will be considered.

IV. DIRECTION OF PROPAGATION AND DOPPLER SHIFT

The direction of propagation of the upstream ion waves was first studied by Anderson et al. [1981]. Anderson's measurements made use of spacecraft spin modulation, not interference patterns. The measurements were difficult to make because the intensity often fluctuates rapidly when compared to the spin period. The ion waves are also observed to shift in direction sometimes on the order of a few tenths of a second, much less than the few seconds required to determine spin modulation. When the measurements of the direction of propagation could be made it was concluded, except for a few anomalous cases, that the peak amplitudes in the electric field were usually aligned parallel to the ambient magnetic field [Anderson et al., 1981].

By using spin-modulated interference patterns in the wave data, the wave vector direction projected into the spin plane can be determined very accurately. The projected wave vector direction can then be compared to the magnetic field direction projected into the spin plane.

In order to determine the wave vector direction the angle between the antenna and some reference point is required. The reference point used is the sun. The sun-antenna angle is an engineering parameter which can be obtained from the data tape. First, one must determine the time of minimum (or maximum) frequency of an interference pattern. The minimum frequency of the interference pattern occurs when the

antenna is oriented parallel to the wave vector projected into the spin plane (or perpendicular to the wave vector direction in the case of the maximum in frequency) as demonstrated in Figure 7. The sun-antenna angle for the minimum in frequency is the sun-wave vector angle. The magnetic field-sun angle is determined by interpolation of high resolution magnetic field data obtained from the magnetometer on ISEE-1 and provided by C. Russell. The sun-wave vector angle is then compared to the sun-magnetic field angle. If the wave vector is parallel to the magnetic field, then the difference of the sun-wave vector angle and the sun-magnetic field angle should always be near zero. Projection effects due to the lack of knowledge of the perpendicular component of the wave vector cause ambiguous results if the wave vector is not parallel to the magnetic field. In order to reduce the problem of projection effects, events were selected when the spacecraft z component of the magnetic field was very nearly zero.

The wave vector direction was determined using interference patterns observed at two different time periods, November 8, 1977, 20^h 12^m to 20^h 27^m and November 23, 1977, 8^h 14^m to 8^h 20^m. A total of 88 separate interference patterns were studied. The results of the study of these time periods indicate that the wave vector direction is not simply aligned parallel to the magnetic field. The distribution of angles between the projected magnetic field for November 23, 1977, 8^h 14^m to 8^h 20^m is given in Figure 8a. The angle between the spin plane projected wave vector and the spin plane projected magnetic field is not observed to be near zero. Out of the 88 interference patterns studied, eight cases coincided with times when the magnitude of the

spacecraft z component of the magnetic field was less than 1% of the total magnitude of the magnetic field. The distribution of angles for the eight events is presented in Figure 8b. The lack of large angles between the spin plane projected wave vector and the magnetic field in Figure 8b indicates that the wave vector is also not perpendicular to the magnetic field. A more detailed example of the geometry for a particular event on November 8, 1977, at 20^h 27^m 33.4^s is illustrated in Figure 9. On November 8, 1977, 20^h 27^m 33.4^s the angle between the wave vector and the magnetic field was 39 degrees. At this time, the spacecraft z component of the magnetic field from the magnetometer data was less than 3% of the total magnitude of the magnetic field. If the wave vector was perpendicular to the magnetic field, then the z component of the wave vector would have to be extremely large to account for the projection of the wave vector onto the spin plane to be at such a small angle to the magnetic field.

Typical values of the angle between the spin plane projected magnetic field and the spin plane projected wave vector range from 10 degrees to 75 degrees and usually average $40^\circ \pm 20^\circ$. This result disagrees with propagation parallel to the magnetic field reported by Anderson et al. [1981]. The reason for this disagreement is not known in detail, but is probably caused by the large fluctuations in frequency of the ion waves and difficulties inherent with the method used by Anderson et al.

In addition to measurements of the direction of propagation, the Doppler shift of the ion waves in the upstream region can be readily measured using the interference patterns observed in the wave data. A

measurement of the rest frame frequency of the waves can be obtained by subtracting the Doppler shift from the frequency measured by the spacecraft.

To determine the Doppler shift of a wave the relation between the observed frequency of the waves and the wavelength of the wave is required. To understand the frequency-wavelength correspondence, consider the equation for the Doppler shift (Equation 9) in detail.

$$\omega'(\vec{k}) = \omega_0(\vec{k}) + \vec{k} \cdot \vec{V}_{SW} \quad , \quad (9)$$

In Equation 9 there are three terms. Each term has certain very important properties. The first term, $\omega'(\vec{k})$ is simply the frequency observed on the wideband frequency-time spectrogram. The observed frequency depends on the wave vector through the rest frame frequency and the Doppler shift. The second term, $\omega_0(\vec{k})$ is the rest frame frequency. The rest frame frequency depends on the wave vector through the dispersion relation for the waves. The dispersion relation depends on the plasma wave mode. Since the mode of propagation of the ion waves has not been conclusively identified, the wave vector dependence of $\omega_0(\vec{k})$ is not known. The third term in Equation 9 is the Doppler shift term. It depends on the magnitude of the wave vector and the direction of propagation relative to the solar wind. This third term can be calculated using information obtained from the interference patterns observed in the wideband data. To determine the Doppler shift, note first that when interference patterns are analyzed, only wave

magnitudes and directions projected into the spin plane are obtained. No information can be obtained about the contribution of the $k_z V_{swz}$ term to the Doppler shift in Equation 9. Fortunately, the solar wind velocity is always very close to the antisunward direction. Since the spin axis of ISEE-1 is perpendicular to the ecliptic plane, the solar wind is rarely more than one degree out of the spacecraft spin plane, therefore $V_{swz} \approx 0$. This simplifies the Doppler shift equation to

$$\omega(\vec{k}) = \omega_0(\vec{k}) + \vec{k}_\rho \cdot \vec{V}_{sw\rho} \quad (10)$$

where k_ρ is the spin plane projected wave vector. Because $|\vec{k}_\rho|$ and the angle between \vec{k}_ρ and $\vec{V}_{sw\rho}$ can be measured at the nulls in the interference pattern, the Doppler shift for these wave vectors can be computed exactly.

In order to determine the Doppler shift, the frequency and time of occurrence of a null in the wideband spectrum for a particular interference pattern is determined, as in Figures 4 and 6. The projected wave vector for the null in intensity is given by Equation 7 to be

$$k_\rho = \frac{2m\pi}{L \cos \phi} \quad (11)$$

This projected wave vector depends only on the antenna length and the direction of the projected wave vector relative to the antenna. When

the antenna is aligned along the projected wave vector as in Figure 7, then ϕ is zero so that

$$k_{\rho\text{Null}} = \frac{2m\pi}{L} \quad , \quad m = 2, 4, \dots \quad . \quad (12)$$

The equation for the frequency of these projected wave vectors is then

$$\omega'(\vec{k}) = \omega_0(\vec{k}) + \frac{2m\pi}{L} |\vec{V}_{\text{sw}}| \cos \psi \quad , \quad m = 2, 4, \dots \quad . \quad (13)$$

Similarly, the Doppler shift equation for a maximum in intensity, obtained from Equations 8 and 10, is

$$\omega'(\vec{k}) = \omega_0(\vec{k}) + \frac{2m\pi}{L} |\vec{V}_{\text{sw}}| \cos \psi \quad , \quad m = 1, 3, 5, \dots \quad . \quad (14)$$

The angle ψ between the projected wave vector and the solar wind can be obtained by measuring the time of the minimum in frequency of the interference pattern exactly the same way as the direction was obtained for the measurements of the direction of propagation.

Since all quantities in either Equations 12 or 13, except for the rest frame frequency, are known for a particular value of m , the rest frame frequency can be calculated. If enough nulls or maximums at different frequencies are observed, one can experimentally determine the dispersion relation for certain specific wave vectors. The dispersion relation cannot be determined completely because the component of the wave vector perpendicular to the spin plane is not known.

The event selected to illustrate the determination of the dispersion relation occurred on November 22, 1977, at 6^h 44^m 15^s. At this time ISEE-1 was located in the upstream region at about 16.8 R_E and 10.3 hours magnetic local time. Figure 6 is an equatorial projection of the ISEE-1 orbit for this day. The particular event at 6^h 44^m was chosen because the antenna interference patterns in the wideband data very clearly show the nulls in intensity at three different frequencies and the maximums in intensity at three frequencies. The identification of the three nulls in intensity is shown in Figure 4.

The nulls and maximums in intensity and the time of occurrence of the nulls and maximums were not measured from the wideband film. The limited dynamic range of the wideband film (at best 20 db) and the difficulty in determining precise times and frequencies cause uncertainties which would be too large to make measurements of the rest frame frequency meaningful. Instead, electric field intensity versus frequency plots of the original digitized wideband data were made at 50 millisecond intervals by computer to reproduce the event with much more accuracy in time and frequency. An example of the intensity versus frequency computer plots centered around 6^h 44^m 17.9^s is presented in Figure 10. The nulls corresponding to $k_{\perp\text{Null}} = \frac{4\pi}{L}$ and $k_{\rho\text{Null}} = \frac{8\pi}{L}$ are identified. The particular geometry for the event obtained from the study of the computer generated plots of the event is illustrated in Figure 11. The solar wind velocity on November 22, 1977, at 6^h 44^m was 307 km/sec [W. C. Feldman, personal communication, 1983]. The results from the study of this event are presented in Table 1. The fact that the rest frame frequencies are negative indicates that the wave is

propagating in the sunward direction, opposite the solar wind velocity. The uncertainty in the rest frame frequencies are a result of a $\pm 6^\circ$ uncertainty in the direction of the spin plane projected wave vector, an uncertainty of ± 1 kHz in the observed frequency, and an uncertainty of ± 5 km/sec in the solar wind velocity. The uncertainty in determining the frequency of the nulls and the maximums and their time of occurrence must be minimized because small uncertainties in the observed frequency or the Doppler-shifted frequency cause large uncertainties in the rest frame frequency. The ion plasma frequency at 6^h 44^m was computed from the observed electron plasma frequency to be about 800 Hz. The rest frame frequencies listed in Table 1 are on the order of the ion plasma frequency. This result, along with the wave vector direction and magnitude observations, is summarized in the next section and used to identify the plasma wave mode.

V. INTERPRETATION

The results of the study of interference patterns in the wide-band data place important constraints on any theory used to explain the production of the ion waves in the upstream region. The results can be summarized as follows:

1. The wavelength of the ion waves is on the order of $2\pi \lambda_{De}$.
2. The wave vector of the ion waves is neither parallel nor perpendicular to the magnetic field. The ion waves are observed to be propagating at an average angle of $40^\circ \pm 20^\circ$ from the magnetic field. The wave vector direction is the same for all frequencies.
3. The wave vectors of the ion waves are directed toward the sun, in the same direction as the ions reflected from the bow shock.
4. The ion waves are Doppler shifted by the solar wind into a frequency range of 1 - 10 kHz. The rest frame frequency increases with increasing wave vector magnitude. The maximum rest frame frequency is on the order of the ion plasma frequency.

The above four results can be used to rule out a number of plasma wave modes. Buneman waves [Rodriguez, 1981] can be ruled out because the wavelengths required are many times the Debye length and would not produce antenna interference patterns in the ISEE-1 data. Bernstein waves can be shown to be heavily damped for angles other than nearly perpendicular propagation. Waves excited by the density gradients [Wu

et al., 1982] have the correct frequency, but these waves propagate perpendicular to the magnetic field and have wavelengths many times the Debye length, which is not consistent with the observational results of this study. Whistler mode waves are observed in the upstream region at frequencies up to about 200 Hz, which is on the order of the ion plasma frequency, [Smith et al., 1967; Anderson et al., 1981]. However, whistler mode waves have wavelengths many times the Debye length and would not produce interference patterns in the wideband data.

The wave mode that fits all observations is the ion acoustic mode. Ion acoustic waves are characterized by short wavelengths, $\lambda \gtrsim 2\pi \lambda_{De}$, which agrees with the short wavelengths observed. Ion acoustic waves have frequencies $\omega < \omega_{pi}$, which agrees with the rest frame frequencies listed in Table 1. For very long wavelengths, the phase velocity of the ion acoustic waves is $\omega/k = C_s$, where $C_s = \sqrt{\frac{kT_e}{m_i}}$ is called the ion acoustic speed. For the event on November 22, 1977, the electron temperature was 1.6×10^5 K [W. C. Feldman, personal communication, 1983]. The ion acoustic speed for this event is then $C_s = 36$ km/sec. Considering the first entry in Table 1, $f_0 = 330$ Hz and $k_\rho = .0292 \text{ m}^{-1}$, the measured phase velocity is $\frac{\omega_0}{k_\rho} = 70$ km/sec, which is about a factor of 2 larger than the ion acoustic speed. The measured phase velocity is expected to be greater than the ion acoustic speed because to obtain the phase velocity the rest frame frequency is divided by k_ρ and not $k = \sqrt{k_\rho^2 + k_z^2}$. Ion acoustic waves can propagate at angles to the magnetic field [Tidman and Krall, 1971], so the measurements of the direction of propagation in this study are not inconsistent with the identification of the upstream ion waves as ion acoustic waves. The next

step is to compare the dispersion relation for ion acoustic waves with the computed rest frame frequencies and wave vectors listed in Table 1.

Krall and Trivelpiece [1973] derived a relationship between frequency and wave number for ion acoustic waves. The derivation uses linear Vlasov theory with Maxwellian velocity distributions and assumes weak damping. The dispersion relation is

$$\omega^2 = \frac{k^2 C_s^2}{1 + k^2 \lambda_{De}^2} \quad (15)$$

where $C_s = \sqrt{\frac{kT_e}{m_i}}$, is the ion acoustic speed. For long wavelengths, $k\lambda_{De} \ll 1$, Equation 15 becomes

$$\omega^2 = k^2 C_s^2 \quad . \quad (16)$$

That is, all waves travel at the ion acoustic speed. For very short wavelengths, $k\lambda_{De} \gg 1$, Equation 15 becomes

$$\omega^2 = \frac{C_s^2}{\lambda_{De}^2} = \omega_{pi}^2 \quad . \quad (17)$$

The fact that $\omega < \omega_{pi}$ suggests normalization of Equation 15 by the ion plasma frequency to get the normalized dispersion relation

$$\frac{\omega^2}{\omega_{pi}^2} = \frac{k^2 \lambda_{De}^2}{1 + k^2 \lambda_{De}^2} \quad (18)$$

To compare this dispersion relation to the quantities listed in Table 1, the value of k_z must be known. This quantity cannot be found using interference patterns. However, it was shown that the wave vector direction is independent of frequency. From this result, one can write

$$k_z = k_\rho \tan \theta \quad , \quad (19)$$

where θ is the angle that the wave vector makes with respect to the spacecraft spin plane. Equation 18 can now be rewritten as

$$\frac{\omega^2}{\omega_{pi}^2} = \frac{k_\rho^2 \lambda_{De}^2 \sqrt{1 + \tan^2 \theta}}{1 + k_\rho^2 \lambda_{De}^2 \sqrt{1 + \tan^2 \theta}} \quad (20)$$

A plot of ω/ω_{pi} versus $k_\rho \lambda_{De}$ for various values of θ is presented in Figure 12.

Also in Figure 12 are the wave number-rest frame frequency points listed in Table 1. In order to normalize the observed values of rest frame frequency and projected magnitude of the wave vector, the Debye length and the ion plasma frequency on November 22, 1977, were calculated from the electron temperature and number density provided by W. C. Feldman. From Figure 12 one can see that the observed frequencies

and projected wave vectors fit the ion acoustic dispersion relation if one assumes that the wave vector is 60° out of the spin plane. The close agreement of the observed data with the characteristic shape of the ion acoustic dispersion relation is a strong indication that the ion waves observed upstream of the Earth's bow shock are ion acoustic waves.

VI. DISCUSSION AND CONCLUSIONS

The final result of this study is that the waves observed in the region upstream of Earth's bow shock in the frequency range from 1 to 10 kHz are Doppler-shifted ion acoustic waves. This result is the same conclusion reached by Gurnett and Frank [1978] and Anderson et al., [1981]; however, the evidence is now much stronger. The work by Anderson et al. used the same data but different methods to arrive at wavelength and measurements of the direction of propagation. This study used more powerful methods to determine the wave vector direction and wavelength and went beyond the studies of Gurnett and Frank and of Anderson et al. by determining the frequency range and general shape of the dispersion curve. Along with the results of the studies of Gurnett and Frank and of Anderson et al., this study now adds overwhelming evidence in favor of ion acoustic waves.

With the results of this study the production of ion acoustic waves by an ion beam instability must be reconsidered. Using Figures 2 and 3 from Lemons et al. [1979], Gary [1981] notes that an ion beam drives the ion acoustic instability with the wave vector parallel to the magnetic field only if $3 < v_b/v_i < 10$ and $T_e/T_i > 5$, where v_b is the velocity of the beam and v_i is the ion thermal velocity. However, the wave vector has now been shown to be at a substantial angle to the magnetic field. To account for propagation at angles to the magnetic field, it can be shown using linear Vlasov theory that v_b is replaced

by $v_b \cos \theta$ [Tidman and Krall, 1971], where θ is the angle between the wave vector and the magnetic field. The wave vector direction can now be adjusted so that the condition $3 < v_b \frac{\cos \theta}{v_i} < 10$ is met. For typical values, $v_b \approx 400$ km/sec and $v_i \approx 20$ km/sec, given by Gary [1981] the minimum angle is $\theta_{\min} = 60^\circ$ which is not inconsistent with the directions of propagation found in this study. This calculation does not demonstrate instability because the other condition, $T_e/T_i > 5$, is not observed in the upstream region. However, the fact that the wave vector is not parallel to the magnetic field improves the possibility of generation of the ion waves in the upstream region by the ion beam instability. It has now been shown that the ion waves in the upstream region are propagating in the same direction as the ions reflected from the bow shock, as predicted by an ion beam instability.

The new measurements of the direction of propagation of the ion waves do not rule out the possibility of generation of ion waves by the heat flux instability [Forsslund, 1970]. Tidman and Krall [1971] show that the heat flux instability occurs for wave numbers such that $\frac{\omega}{k} < v_b \cos \theta$. This condition produces a cone of unstable phase velocity vectors centered around the magnetic field. As discussed by Gurnett and Frank [1978] if the net current is zero in the solar wind the presence of an ion beam produces a shift between the electrons and solar wind ions very similar to the heat flux instability. This mechanism also produces wave vectors directed toward the sun, in agreement with observations. However, the heat flux type of instabilities also require a relatively large T_e/T_i ratio, which is usually not observed in the upstream region.

In summary, the results of this study answer some important questions and open up possibilities of new approaches to the important question of the generation of ion acoustic waves in the solar wind. The methods used in this study are limited to wavelengths shorter than the spacecraft antenna length. It is possible that this method of analysis may be applicable to other types of waves found in the solar wind and the terrestrial magnetosphere.

Table 1

Observed and Calculated Frequencies for
November 22, 1977, 6^h 44^m 18^s

m	Wave No. (m^{-1})	Observed Frequency kHz	Doppler Shift kHz	Rest Frame Frequency Hz
1	.0292	$1.1 \pm .1$	-1.43	-330 ± 100
2	.0584	$2.3 \pm .1$	-2.85	-550 ± 110
3	.0877	$3.6 \pm .1$	-4.28	-680 ± 120
4	.1169	$4.9 \pm .1$	-5.70	-800 ± 140
5	.1461	$6.2 \pm .1$	-7.13	-930 ± 160
6	.1753	$7.7 \pm .1$	-8.46	-760 ± 220

ACKNOWLEDGEMENTS

This work was supported by the National Aeronautics and Space Administration through Contract NAS5-26829 with Goddard Spaceflight Center and Grant NGL-16-001-043 with NASA Headquarters, and the Office of Naval Research.

REFERENCES

- Anderson, R. R., C. C. Harvey, M. M. Hoppe, B. T. Tsurutani, T. E. Eastman, and J. Etcheto, Plasma waves near the magnetopause, J. Geophys. Res., 87, 2087-2107, 1982.
- Anderson, R. R., G. K. Parks, T. E. Eastman, D. A. Gurnett, and L. A. Frank, Plasma waves associated with energetic particles streaming into the solar wind from the Earth's bow shock, J. Geophys. Res., 86, 4493-4510, 1981.
- Forslund, D. W., Instabilities associated with heat conduction in the solar wind and their consequences, J. Geophys. Res., 75, 17, 1970.
- Gallagher, D. L., Short wavelength electrostatic waves in the Earth's magnetosheath, Ph.D. Dissertation, University of Iowa, 1982.
- Gallagher, D. L., Short wavelength electrostatic waves in the Earth's magnetosheath, J. Geophys. Res., submitted, 1982.
- Gary, S. P., Ion-acoustic-like instabilities in the solar wind, J. Geophys. Res., 83, 2504, 1978a.
- Gary, S. P., Microinstabilities upstream of the Earth's bow shock: A brief review, J. Geophys. Res., 86, 4331, 1981.
- Gurnett, D. A., and R. R. Anderson, Plasma wave electric fields in the solar wind: Initial results from Helios 1, J. Geophys. Res., 82, 632, 1977.

- Gurnett, D. A., and L. A. Frank, Ion acoustic waves in the solar wind, J. Geophys. Res., 83, 58, 1978.
- Gurnett, D. A., F. L. Scarf, R. W. Fredricks, E. J. Smith, The ISEE-1 and ISEE-2 plasma wave investigation, IEEE Trans. Geosci. Electr., GE-16, 225, 1978.
- Krall, Nicholas A., and Alvin W. Trivelpiece, Principles of Plasma Physics, McGraw-Hill, 1973.
- Lemons, D. S., J. R. Asbridge, S. J. Bame, W. C. Feldman, S. P. Gary, and J. T. Gosling, The source of electrostatic fluctuations in the solar wind, J. Geophys. Res., 84, 2135, 1979.
- Rodriguez, P., Ion waves associated with solar and beam-plasma interactions, J. Geophys. Res., 86, 1279-1289, 1981.
- Scarf, F. L., R. W. Fredricks, L. A. Frank, C. T. Russell, P. J. Coleman, Jr., and M. Neugebauer, Direct correlations of large amplitude waves with suprathermal protons in the upstream solar wind, J. Geophys. Res., 75, 7316, 1970.
- Smith, E. J., R. H. Holzer, M. G. McLeod, and C. T. Russell, Magnetic noise in the magnetosheath in a frequency range 3-300 Hz, J. Geophys. Res., 72, 4803, 1967.
- Temerin, Michael, Doppler shift effects on double-probe measured electric field power spectra, J. Geophys. Res., 84, 5929-5934, 1979.
- Tidman, D. A. and Nicholas A. Krall, Shock Waves in Collisionless Plasmas, Wiley, 1971.

FIGURE CAPTIONS

Figure 1 Wideband data from the ISEE-1 spacecraft on December 24, 1977, (day 358) illustrate the characteristic short wavelength, antenna interference effects on ion waves in the upstream region. The spacecraft was located at about $22 R_E$, and 6.1 hours magnetic local time. The upper panel shows the characteristic shape of the electric field emissions and their relation to the spin of the spacecraft. The lower panel is the wideband data where higher electric field intensities are shown as darker shading. The periodic change in frequency is directly related to the spacecraft spin. The null in intensity between 3 and 4 kHz centered around $17^h 23^m 49^s$ occurs for a specific wave vector.

Figure 2 The geometry used to understand the antenna response to an electrostatic wave. The electric field, \vec{E} and the wave vector, \vec{k} are in the x-z plane. The spacecraft antenna spin axis is in the \hat{z} direction. The terms E_x and k_x are the spin plane projected electric field and wave vector. $E_x \cos \phi$ and $k_x \cos \phi$

are the spin plane projected electric field and wave vector projected onto the antenna.

Figure 3

A comparison of wideband data from the ISEE-1 and -2 spacecraft is displayed. The spacecraft were located in the upstream region about 300 km apart. The upstreaming protons from the bow shock, which are thought to trigger the ion wave instability travel the 300 km in about one second. The general structure of the increase and decrease in frequency observed in the wideband data is the same for the two spacecraft with the exception that ISEE-2 appears to have an overall shift of about one second. However, detailed structure such as the antenna interference patterns centered around 20^h 22^m 15^s for ISEE-1 are absent in the ISEE-2 wideband spectrograms.

Figure 4

Wideband data on November 22, 1977, used to show that the wave vector direction is the same for all frequencies. On November 22, 1977, (day 326) ISEE-1 was located in the upstream region at 10.3 hours magnetic local time and at a distance of about 16.8 R_E. Notice the sharp division between the interference patterns identified by the arrow at about 6^h 44^m 17.3^s. This sharp division at all frequencies indicates that the direction of the wave vector is the same for all frequencies. This event is used for the

calculation of the Doppler shift of the ion waves. The nulls identified and their time of occurrence give the frequency-wave vector relationship required for the equation for the Doppler shift.

Figure 5

ISEE-1 wideband frequency-time spectrogram showing the effect of the Doppler shift on the interference patterns observed in the upstream region. On November 23, 1977, at 8^h 19^m 14^s ISEE-1 was located in the upstream region at a radial distance of 19.8 R_E. Starting at 8^h 19^m 14^s, the bottom of the interference pattern marked by a horizontal bar is at about 4 KHz. At 8^h 19^m 16^s, the bottom of the interference pattern has shifted downward about 500 Hz. At 18.5^s the lower portion of the interference pattern has dropped to about 3 kHz and one half spacecraft rotation later at 20.1^s it is down near 2 kHz. The interference pattern retains its shape, but shifts in frequency as the magnitude of the wave vector or its direction with respect to the solar wind changes.

Figure 6

Wideband spectra for ISEE-1 at two different times on day 326 are shown superimposed on an equatorial projection of the ISEE-1 orbit. At 6^h 56^m ISEE-1 is located near the bow shock in the upstream region.

The ion waves are observed to have Doppler shifts of up to 10 kHz. At this time the solar wind velocity is about 300 km/sec and directed almost antisunward. The spectrogram starting at 9^h 25^m 26^s was taken when ISEE-1 was in the outer magnetosheath close to the bow shock. The Doppler-shifted waves extend up to about 4 kHz because at this time the plasma bulk flow velocity is only about 160 km/sec, a little over half that of the solar wind.

Figure 7

Illustration of the method of determining the spin plane projected direction of propagation of the ion waves when interference patterns are observed in the wideband data. The time t_0 in the wideband data in the upper left hand corner corresponds to the spin plane projected wave vector aligned along the spacecraft antenna. This antenna-x-axis direction can be determined from the data tape for this time and the direction can be compared to the spin plane projected magnetic field.

Figure 8

Histograms of the observed angle between the spin plane projected wave vector and the spin plane projected magnetic field.

a) The upper panel is a histogram of the 47 separate measurements of the angle between the spin plane projected wave vector and the spin plane projected

magnetic field. If the wave vector were parallel to the magnetic field then the angle between the projected wave vector and the projected magnetic field would always be zero. Because the angle is rarely observed to be zero one can conclude that the wave vector is not parallel to the magnetic field.

b) The lower panel shows 8 events observed on November 8, 1977, from 20^h 12^m to 20^h 27^m when the z component of the magnetic field was zero. If the wave vector were perpendicular to the magnetic field all events would have spin plane projected angle of 90 degrees. Because the angle is not observed to be 90 degrees, one can conclude that the wave vector is not perpendicular to the magnetic field.

Figure 9

An example of the geometry for a particular observed interference pattern on November 8, 1977, at 20^h 27^m 33.4^s. At this time ISEE-1 was located in the upstream region at about 17.1 R_E and 8.4 hours magnetic local time. The spacecraft z component of the magnetic field was very nearly zero for this particular event. The spin plane projected wave vector is 39 degrees from the magnetic field. If the wave vector were perpendicular to the magnetic field then the spacecraft z component of the wave vector would have to be extremely large to account for the small pro-

jected angle relative to the magnetic field. From this example and others like it one can assume that the wave vector is not perpendicular to the magnetic field.

Figure 10

Seven computer generated intensity versus frequency plots centered around $6^{\text{h}} 44^{\text{m}} 17.9^{\text{s}}$. The event illustrated in Figure 4 was reproduced by a total of 80 of these plots spaced at intervals of 50 milliseconds. These 80 computer generated plots were used to determine the observed frequency and time of a particular $k_{\rho\text{Null}}$ with less uncertainty than if the wideband film were used. The two points identified at $6^{\text{h}} 44^{\text{m}} 17.9^{\text{s}}$ were used in the calculation of the Doppler shift of the ion waves.

Figure 11

The geometry for the event in Figure 4. The spin plane projected wave vector direction was determined from the time of minimum in frequency in the wideband data. The solar wind velocity and direction was obtained from the solar wind instrument on ISEE-1 and provided by W. C. Feldman.

Figure 12

The normalized dispersion curve of ion acoustic waves with wave vectors that have propagation angles of 75° , 60° , 30° , and 0° out of the spacecraft spin plane are shown. The x-axis is the magnitude of the

spin plane projected wave vector normalized by the Debye length. The y-axis is the rest frame frequency normalized by the ion plasma frequency. The data points on the graph are the points listed in Table 1, normalized by the Debye length and the ion plasma frequency.

8-083-75

ISEE-1 WIDEBAND DATA

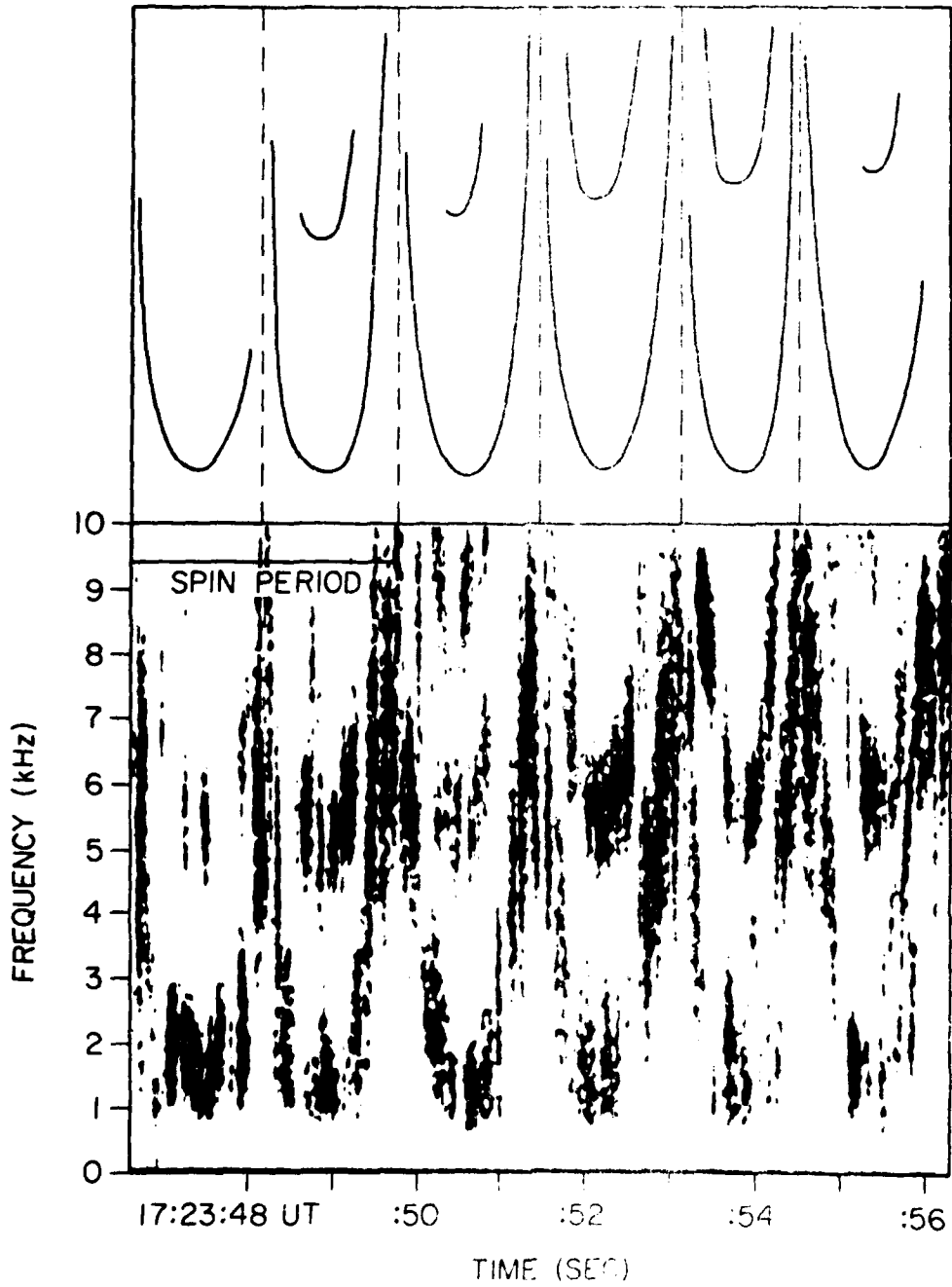


Figure 1

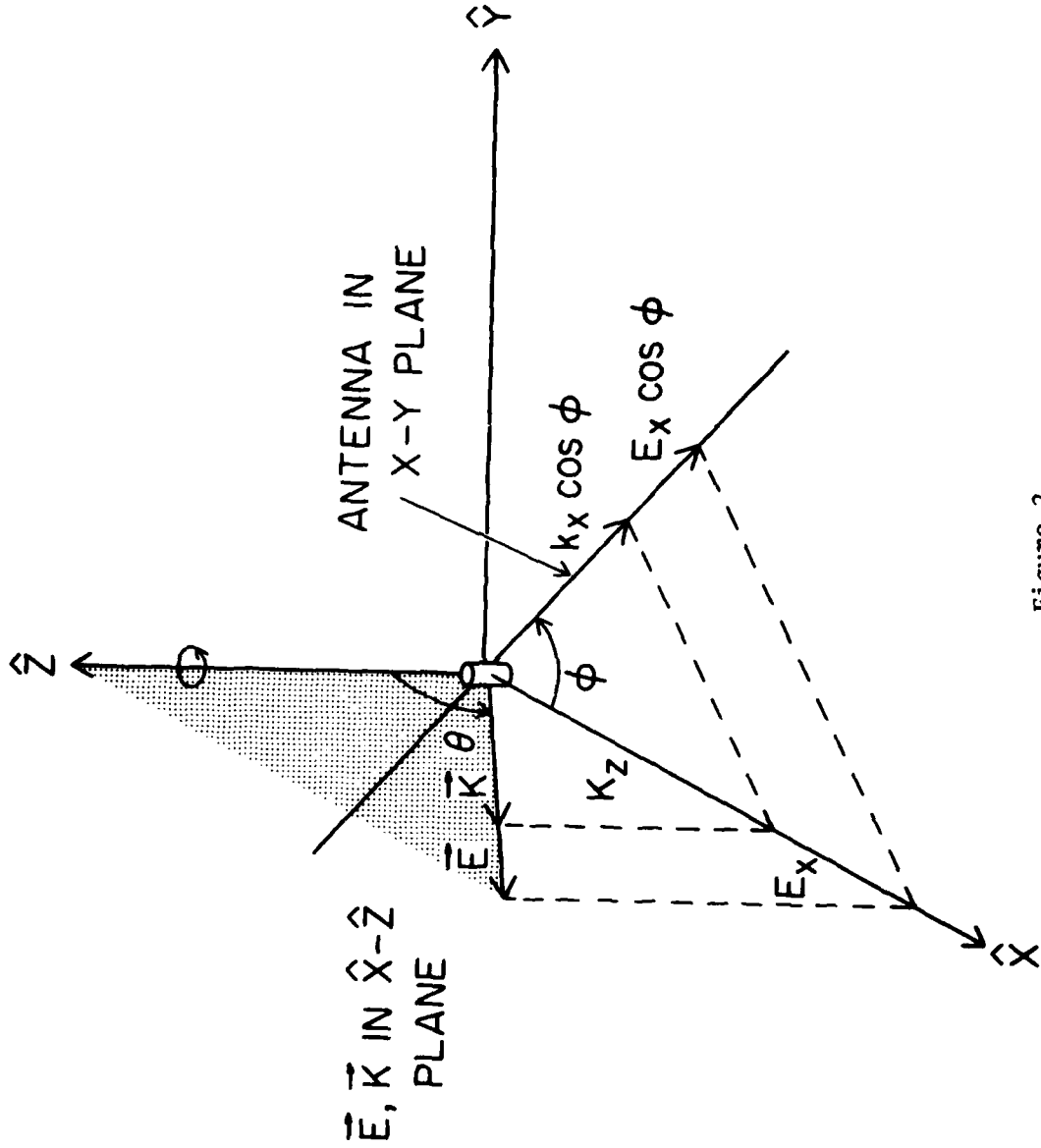


Figure 2

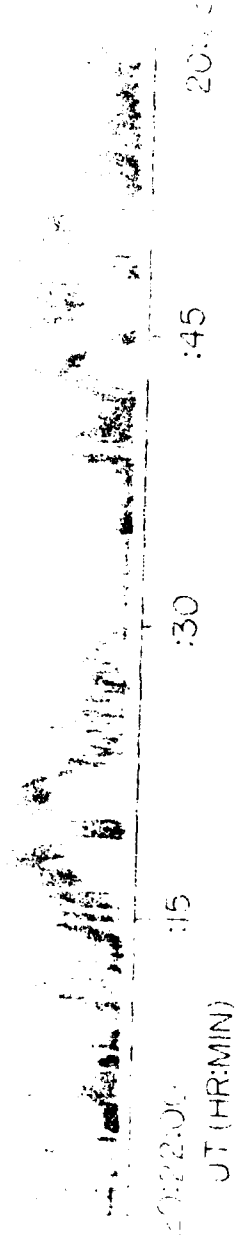


Figure 3

183 146-1

ISEE-1 WIDEBAND DATA
YEAR 1977 DAY 326

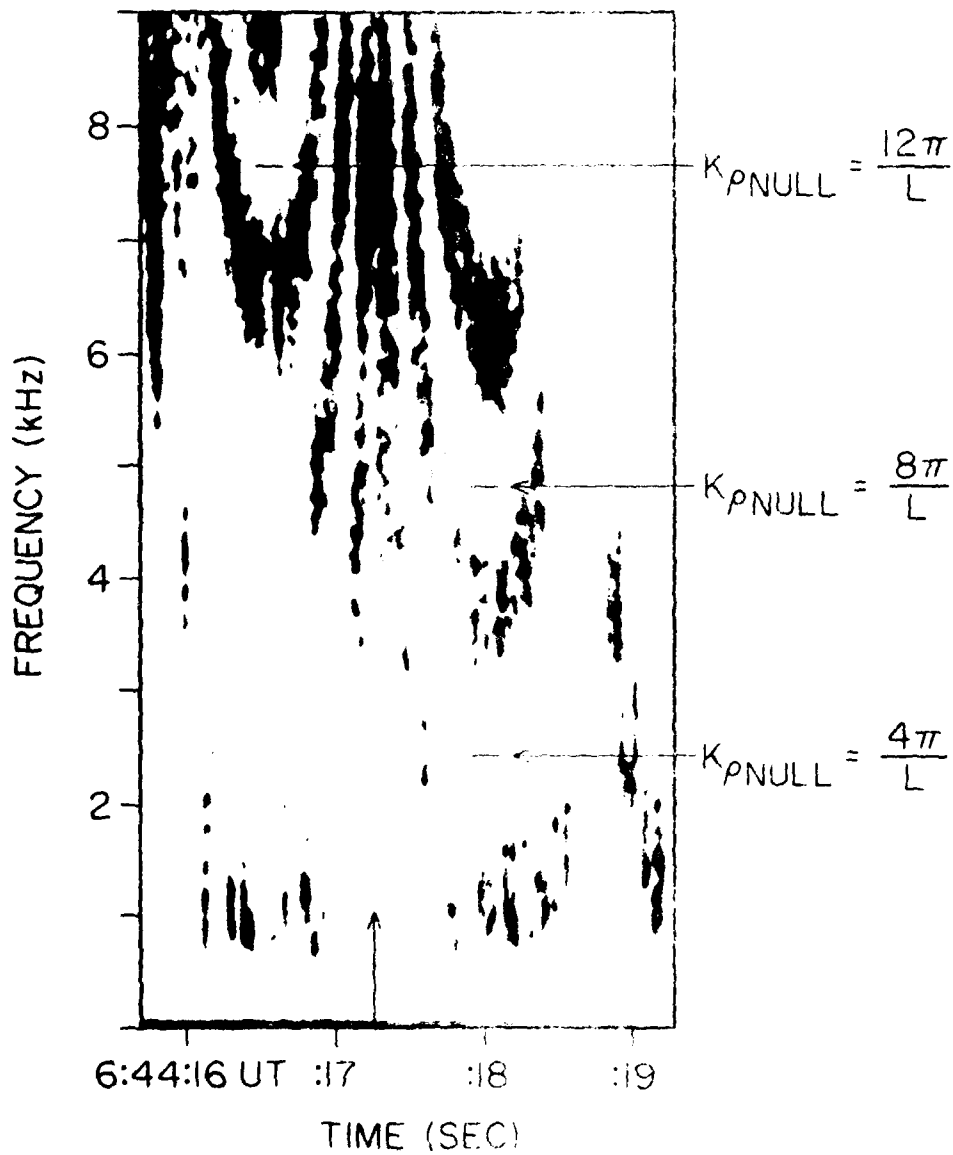


Figure 1

A-683-114

ROTTENBERG AND DATA

NOVEMBER 21, 1967 DAYS 327 ORBIT 13
R = 19.8 R_E MAG LAT = 30.2° MLT = 8.9 HRS

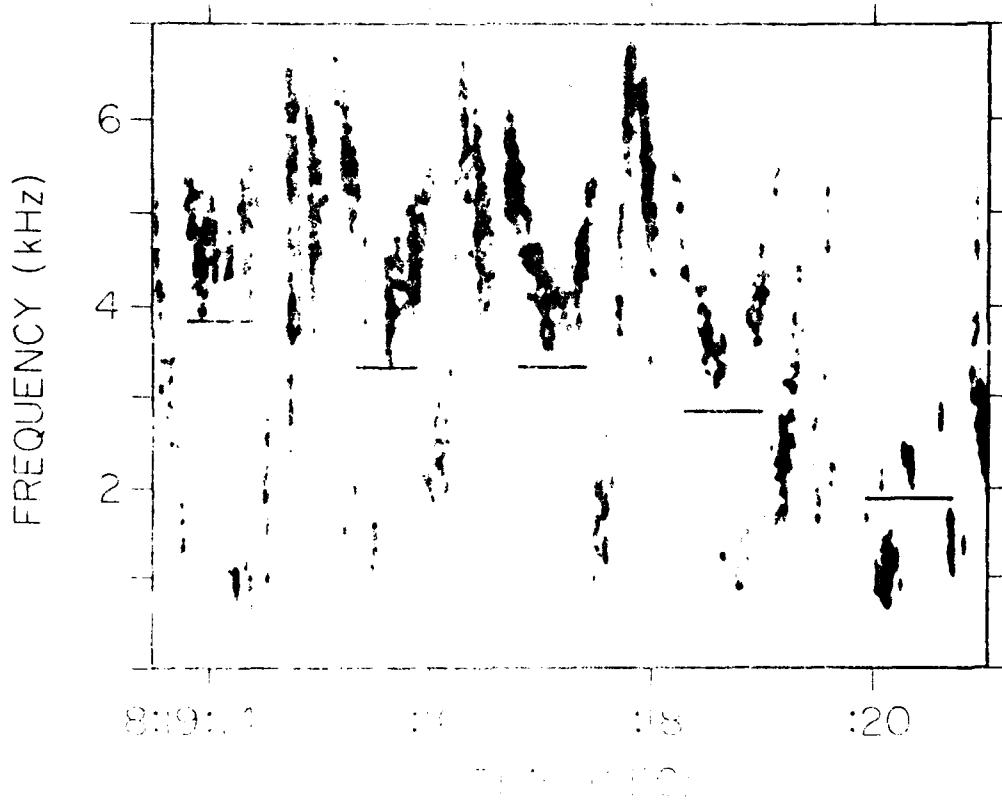


Figure 5

EQUATORIAL PROJECTION OF ISEE 1 ORBIT
 YEAR 1977 DAY 320

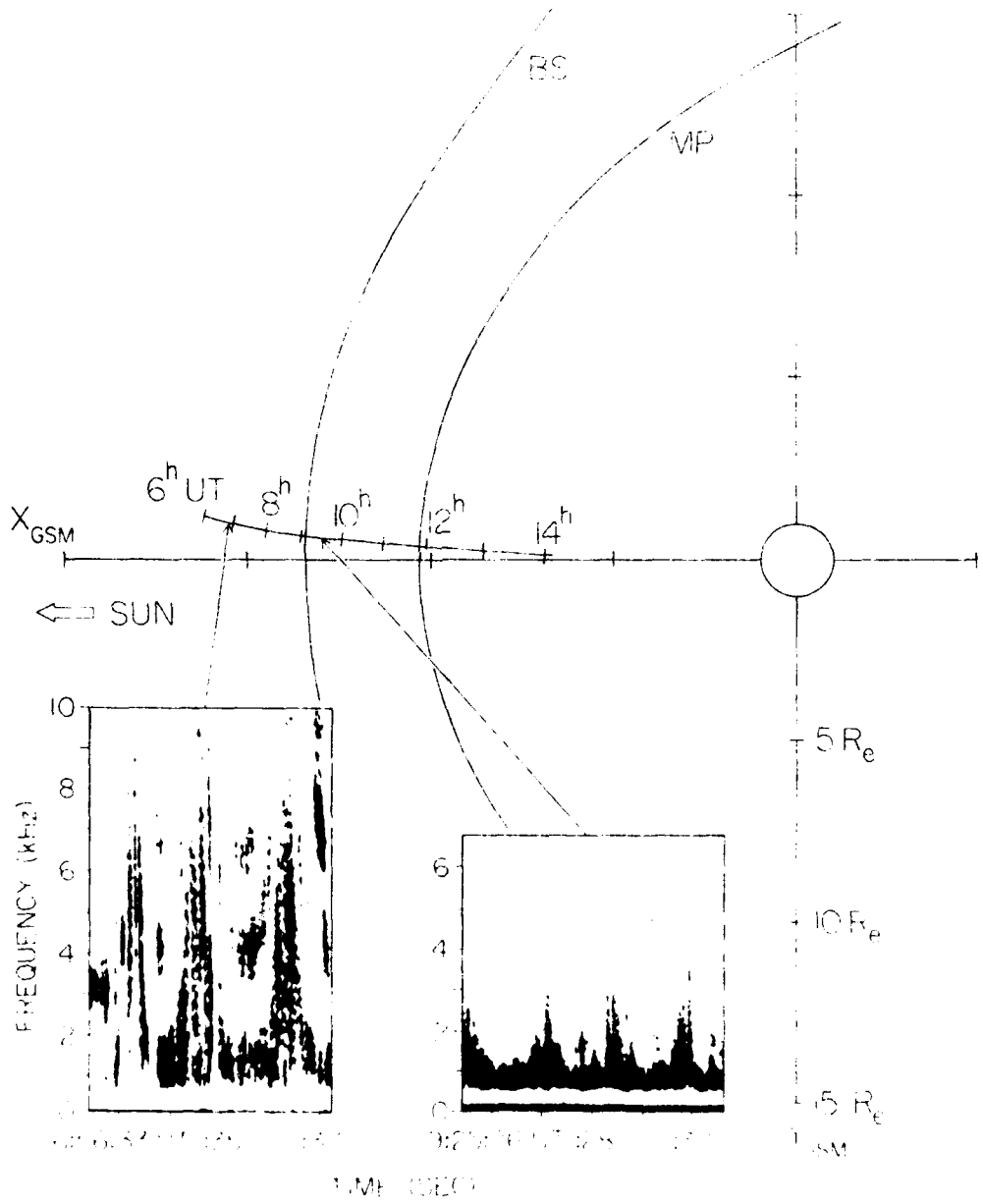
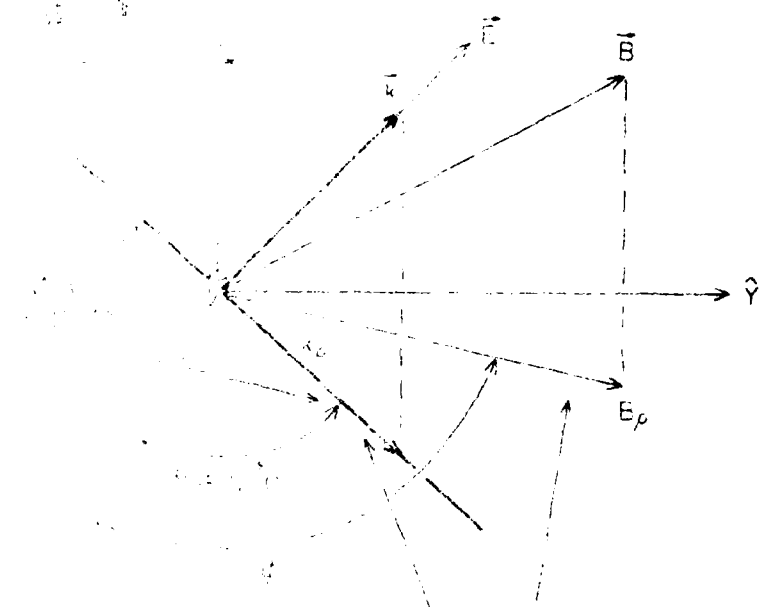


Figure 6

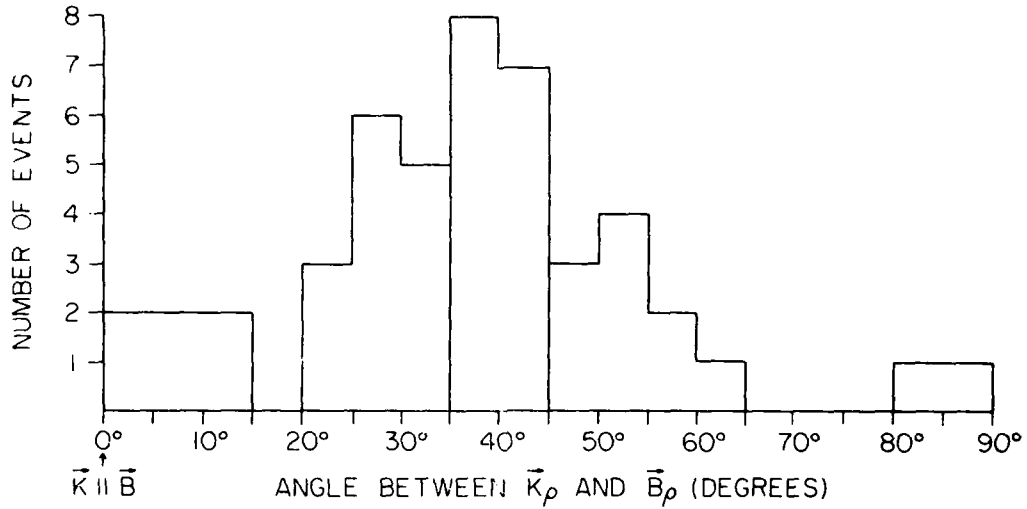
FREQUENCY (kHz)



SPIN PLANE PROJECTED
WAVE NUMBER (k_p)
AND WAVE NO FIELD (B_p)

B-G83-284-1

WAVE VECTOR DIRECTION
 1977 DAY 327 8^h14^m - 8^h20^m



WAVE VECTOR DIRECTION
 1977 DAY 312 20^h17^m - 20^h27^m
 EVENTS WHEN $B_z \approx 0$

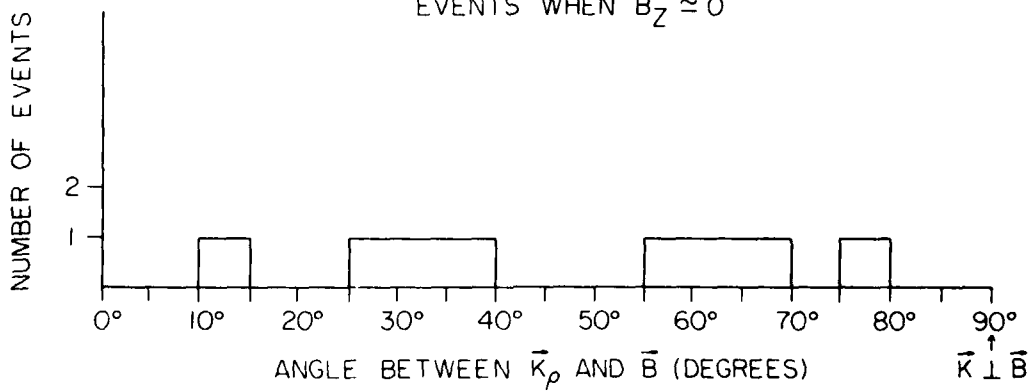
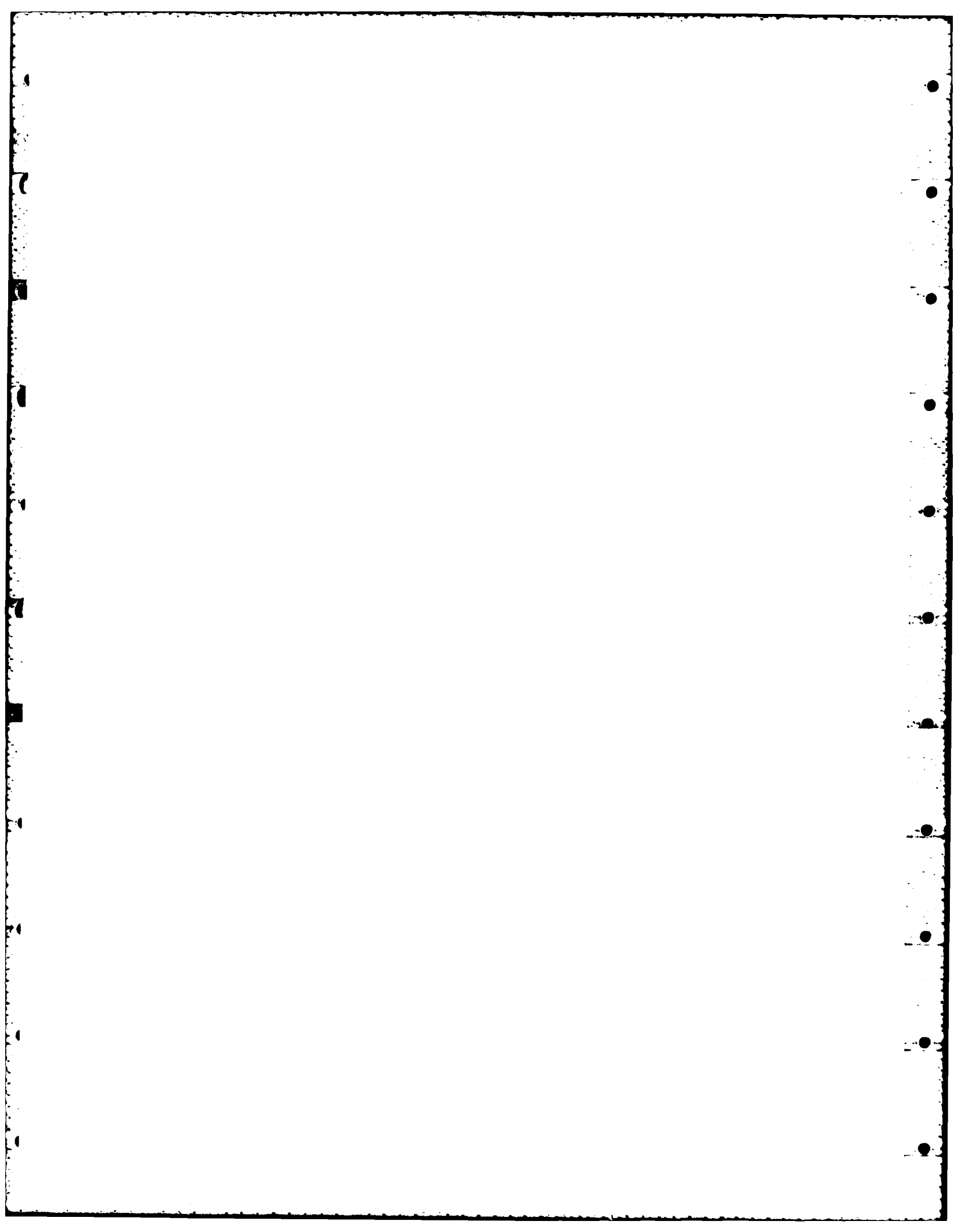


Figure 8



EVENT GEOMETRY FOR
NOVEMBER 8, 1977 20^h 27^m 33^s.4

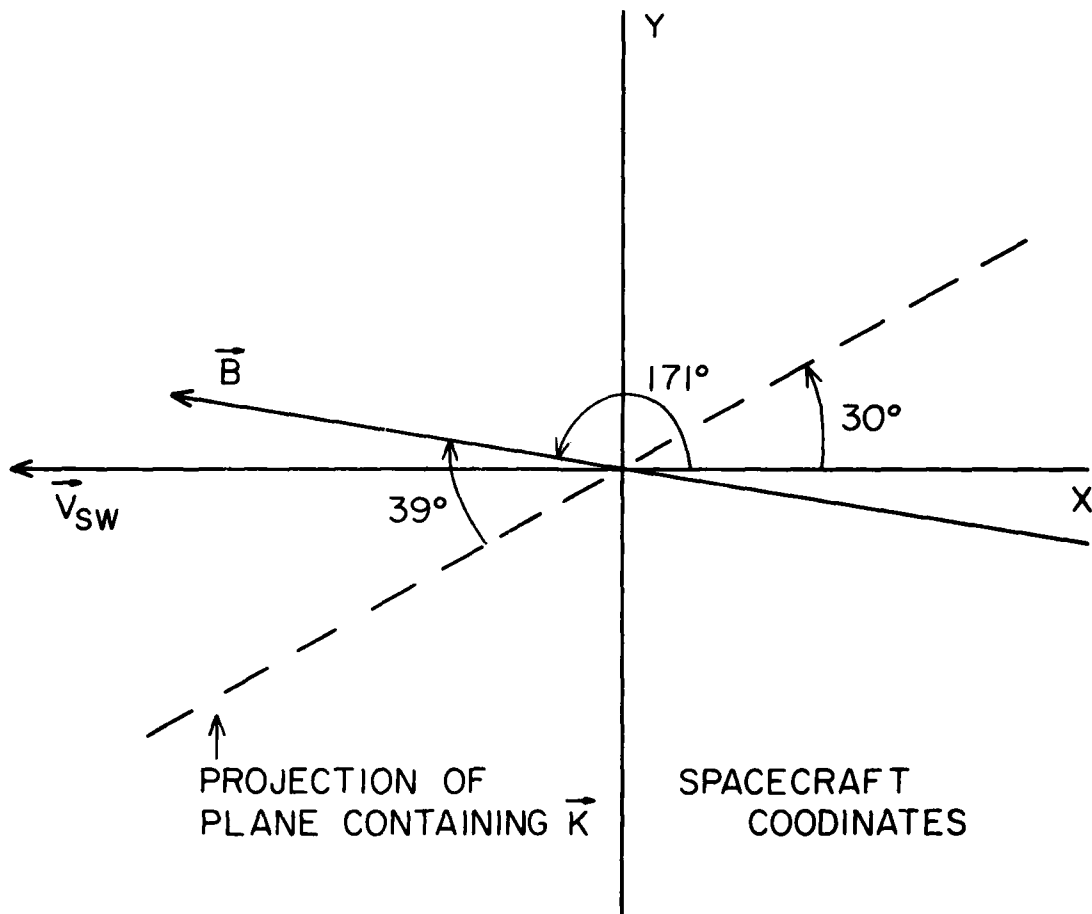


Figure 9

C-683-304-2

ISEE - I INTENSITY -vs- FREQUENCY
NOVEMBER 22, 1977
50 ms/SWEEP

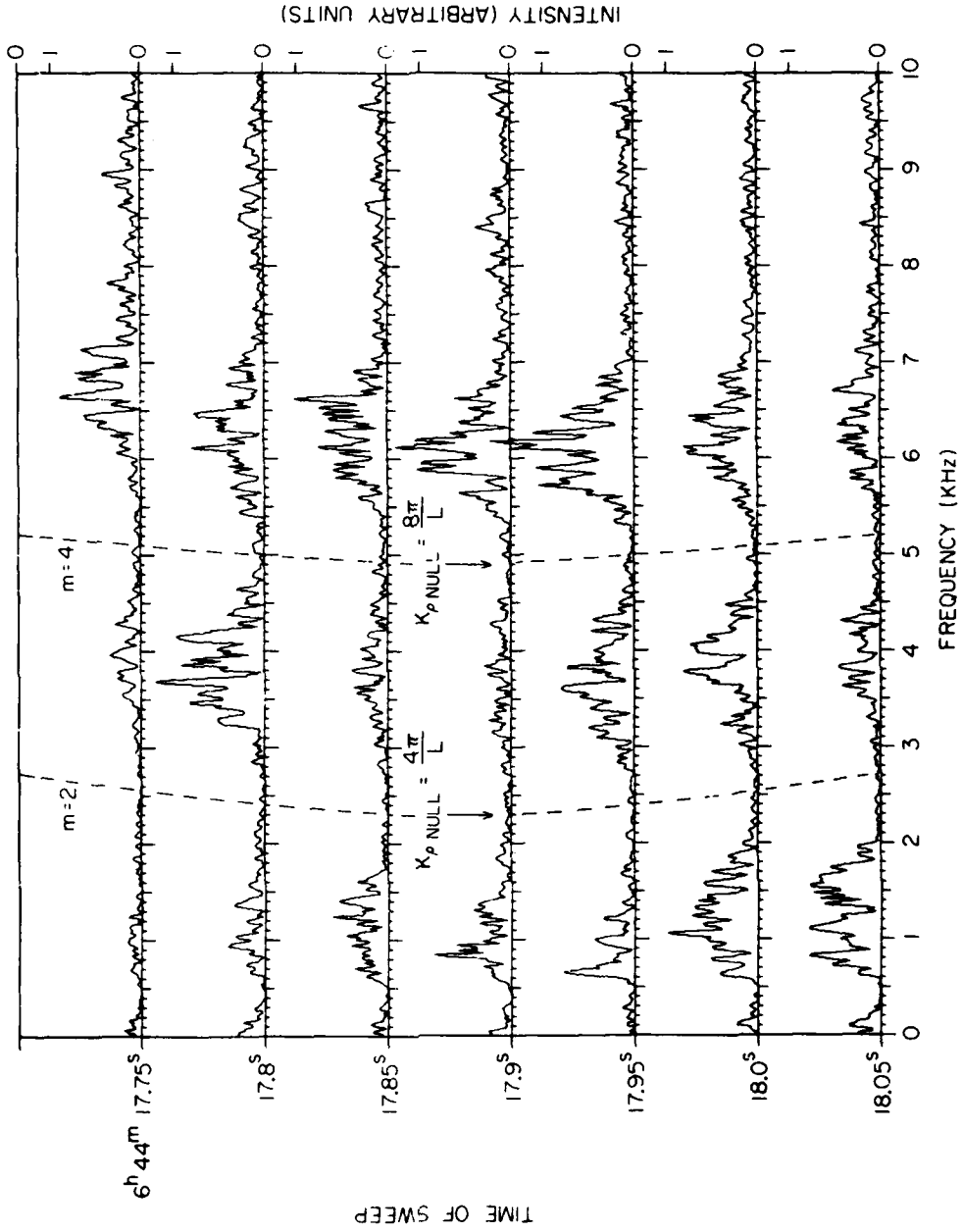


Figure 10

A-G83-219

EVENT GEOMETRY
FOR NOVEMBER 22, 1977 6^h 44^m 17.^s9

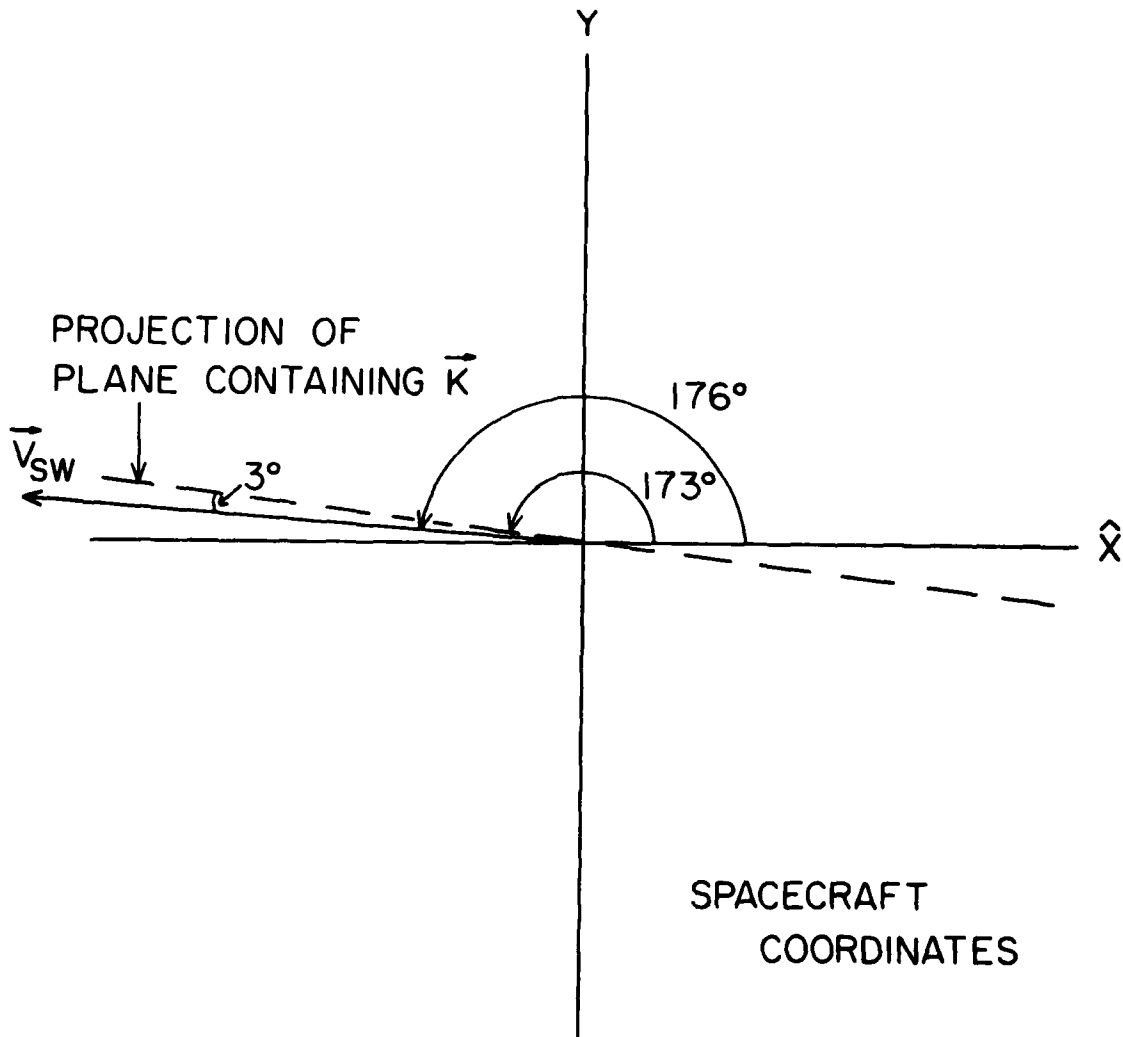


Figure 11

B-G83-233-2

NORMALIZED FREQUENCY VERSUS NORMALIZED WAVE NUMBER
FOR ION ACOUSTIC WAVES

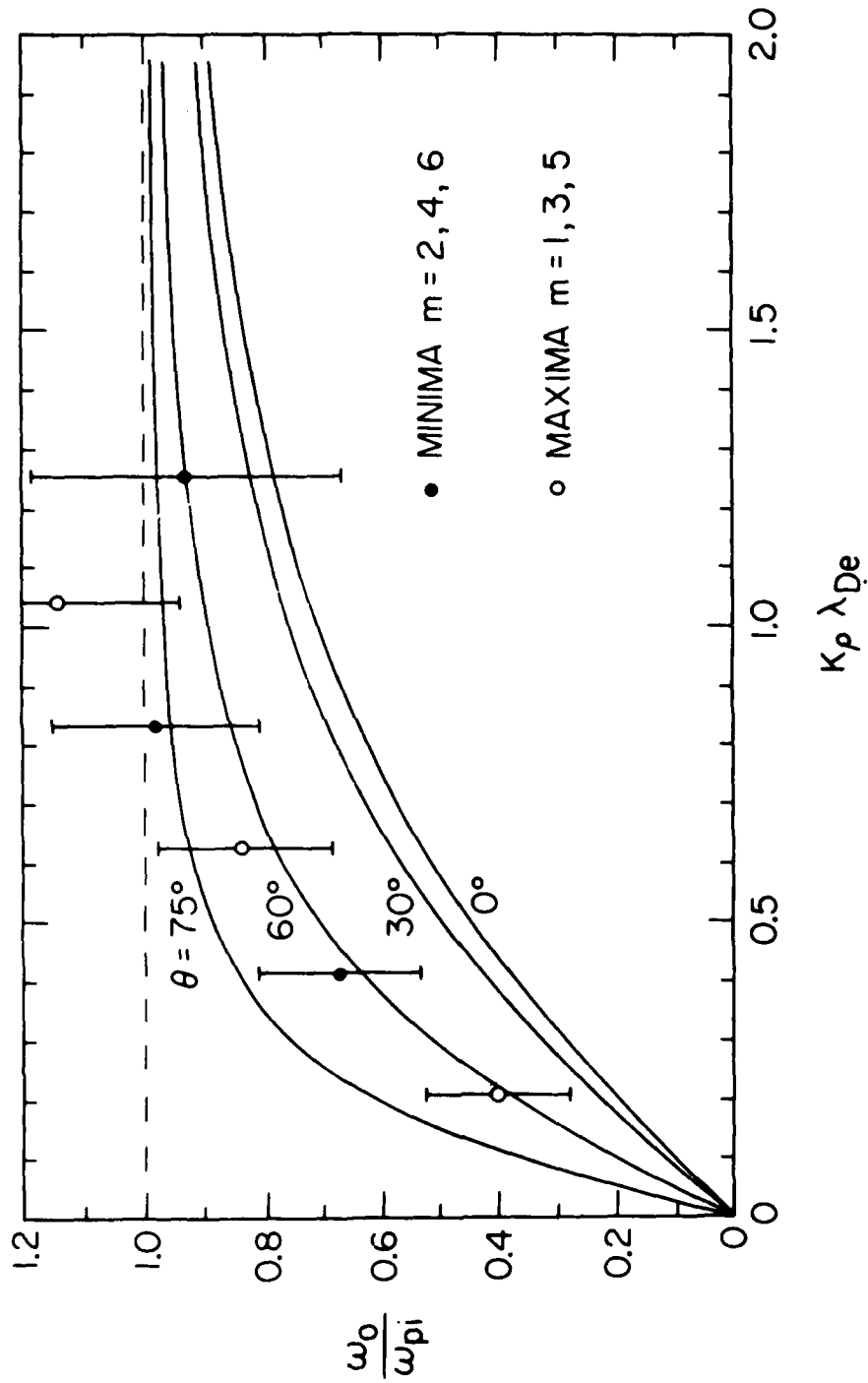


Figure 12

END

FILMED

8-83

DTIC